International Journal of Fluid Machinery and Systems
Vol. 8, No. 1, January-March 2015

DOI: http://dx.doi.org/10.5293/IJFMS.2015.8.1.036
ISSN (Online): 1882-9554

Original Paper

Numerical Analysis of Centrifugal Impeller for Different Viscous Liquids

Sayed Ahmed Imran Bellary and Abdus Samad

Indian Institute of Technology Madras Chennai-36, India
email: ibellary@gmail.com, samad@iitm.ac.in

Abstract

Oil and gas industry pumps viscous fluids and investigation of flow physics is important to understand the machine behavior to deliver such fluids. 3D numerical flow simulation and analysis for different viscous fluids at different rotational speeds of a centrifugal impeller have been reported in this paper. Reynolds-averaged Navier Stokes (RANS) equations were solved and the performance analysis was made. Standard two equation k-ε model was used for the turbulence closure of steady incompressible flow. An inlet recirculation and reverse flow in impeller passage was observed at low impeller speeds. It was also found that the higher viscosity fluids have higher recirculation which hinders the impeller performance.

Keywords: Centrifugal impeller, Off design condition, Rotational speed, Viscosity, Inlet recirculation.

1. Introduction

Three-dimensional internal flow through centrifugal pumps is quite complex and the flow is characterized by diffusion, strong swirl, cavitation, flow separation with reverse flow and recirculation flow at inlet and exit etc. Adverse pressure gradient, inlet recirculation, flow separation in impeller passage and exit recirculation always exists at off-design conditions. Being widely used in downstream, upstream oil industry and many other applications, the pump system requires operation over a wide flow range. In this regard, understanding the performance of impeller at off-design operating conditions becomes imperative.

Performance analysis of the impellers was studied with the help of computational fluid dynamics (CFD) simulations by many researchers [1-5]. Murakami *et al*. [6] measured the flow pattern in centrifugal pump impeller with three and seven blades using a cylindrical yaw probe. They concluded that the velocity and pressure distribution of seven-bladed impeller coincides with the numerical solution whereas three-bladed impeller deviated largely from numerical solutions both at the design and off-design conditions. Liu *et al.* [7], Akhras *et al.* [8] have reported that impeller flow separation was observed on blade surface at off-design flow rate as compared to smooth flow. As reported by researchers [3-5], flow field within impeller passage is highly complex and depends on flow rate, number of blades, blade curvature and specific speed. Abramian and Howard [9] showed that pressure side mean flow separation under low flow condition within impeller passage is affected by a combined effect between a secondary vorticity initiated at the inlet and a potential vortex at impeller exit. Kaupert *et al.* [10] performed off-design performance both by experiment and numerical method. Their experimental result showed the simultaneous appearance of shroud side reverse flow at impeller inlet and outlet but their CFD results could not predict the outlet reverse flow. Tsukamoto *et al.* [11] carried out experiment and validated the predicted results of head-flow curves, diffuser inlet pressure distribution and impeller radial forces numerically over entire flow range and they predicted back flow at small flow rate, but they did not show an exact back flow pattern along the impeller outlet.

Effect of fluids viscosity on centrifugal pump was studied by several authors [12-14]. The nature of flow pattern inside the impeller shows large increase in the disc friction losses over impeller, shroud and hub. It affects the slip coefficient, increases the hydraulic loss and reduces the flow through impeller [12]. Also, the existence of wide wake near the blade suction side of centrifugal impeller was explained by Li [14]. From the experimental results [13], it was shown that the flow patterns near impeller inlet were much affected by the viscosity compared to flow patterns near impeller outlet. Viscosity reduces performance of impeller, by decreasing the efficiency and increasing consumption of power [14-16].

Study of centrifugal pump performance handling different fluids is essential for the design, selection, and operation of the centrifugal pump impeller used in the petroleum industry such as improving oil recovery, upstream and downstream sector, chemical industry and water treatment industry etc. Despite the importance of multicomponent flows, such flows have not been

Received October 16 2014; accepted for publication December 26 2014: Review conducted by Prof. Xuelin Tang. (Paper number O14028C)
Corresponding author: samad@iitm.ac.in

explored to the same extent as gas-liquid and solid-liquid flows were. Knowledge of flow structure, pressure and velocity distribution in the impeller at off-design points could lead to the development of more accurate numerical pump model. Although many researchers [14-16] have demonstrated experimentally and numerically the effect of viscosity on pump performance, but still there is a space to understand detailed pressure and velocity distribution effect on the performance of pump.

In this paper, a study to investigate the performance analysis of a centrifugal pump impeller for four different viscous fluids was performed. Numerical simulations were done at the design and off-design conditions. It was also tried to find the nature, distribution and behavior of velocity and pressure at design and off-design point.

2. MATHEMATICAL DESCRIPTION

2.1 Geometrical model

Table 1 features geometric parameters of impeller with computational model shown in Fig. 1 which was used for the present simulations.

Table 1 Features of impeller

Parameter	Dimension
Shaft diameter, D_s	40 mm
Hub diameter, D_h	55 mm
Inlet diameter, D_1	160 mm
Inlet blade width, b_1	54 mm
Outlet blade width, b_2	30 mm
Inlet blade angle, β_1	23^o
Outlet blade angle, β_2	27^o
Blade number, z	7
Outlet diameter, D_2	365

Numerals 1 and 2 designate the inlet and outlet in the velocity triangle for the blade as shown in Fig. 2. Input shaft power (P) in watt was calculated [17] from the relation:

$$P = \rho g H_{th} Q \tag{1}$$

Hydraulic efficiency is defined [17] in terms of head and hydraulic losses:

$$\eta = \frac{H_a}{H_{th}} = \frac{H_{th} - \Delta H}{H_{th}} = \frac{H_a}{H} \tag{2}$$

As per Euler's equation, head [4] is given by:

$$H_{th} = \frac{c_{u2}u_2 - c_{u1}u_1}{g} \tag{3}$$

Normal entry at impeller inlet implies c_{u1}=0 as in Fig. 2. The Equation (3) becomes:

$$H_{th} = \frac{c_{u2}u_2}{g} \tag{4}$$

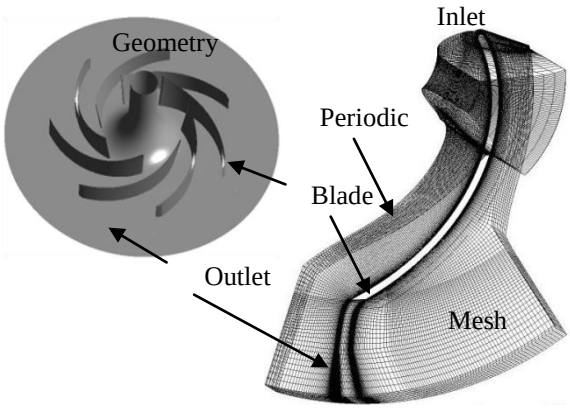

Fig. 1 Geometry and mesh in flow domain

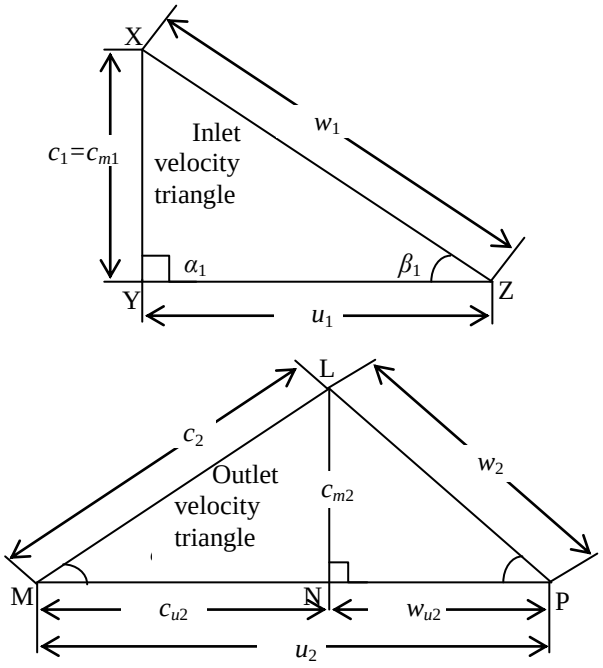

Fig. 2 Velocity triangles

Table 2 represents four different fluids with their respective densities and viscosities. The fluids were used as working fluids for the numerical computations.

Table 2 Viscosity and density of the fluids

Fluid	Viscosity [N-s/m^2]	Density [kg/m^3]
Water	1.002E	997
Crude-oil	5.000E	835
Gasoline	5.000E	720
Kerosene	2.100E	810

2.2 Numerical modeling

CFD tools enable faster geometry modeling, grid generation and solving the mass, momentum and energy equations to speed up the design procedure. In the present work, modeling and meshing of the flow domain were carried out by using ANSYS-BladeGen and Turbogrid module. ANSYS-CFX 13.0 [18] was used for the simulations. The steady, incompressible conditions were applied and RANS equations were solved. The governing equations are given below.

Mass conservation equation;

$$\frac{\partial U}{\partial x}+\frac{\partial V}{\partial y}+\frac{\partial W}{\partial z}=0 \tag{5}$$

Momentum conservation equation;

x-momentum,

$$\rho\left[\frac{\partial U^2}{\partial x}+\frac{\partial UV}{\partial y}+\frac{\partial UW}{\partial z}\right]=-\frac{\partial p}{\partial x}+\mu\left[\frac{\partial^2 U}{\partial x^2}+\frac{\partial^2 U}{\partial y^2}+\frac{\partial^2 U}{\partial z^2}\right] \tag{6}$$

y-momentum,

$$\rho\left[\frac{\partial UV}{\partial x}+\frac{\partial V^2}{\partial y}+\frac{\partial VW}{\partial z}\right]=-\frac{\partial p}{\partial y}+\mu\left[\frac{\partial^2 V}{\partial x^2}+\frac{\partial^2 V}{\partial y^2}+\frac{\partial^2 V}{\partial z^2}\right] \tag{7}$$

z-momentum,

$$\rho\left[\frac{\partial UW}{\partial x}+\frac{\partial VW}{\partial y}+\frac{\partial W^2}{\partial z}\right]=-\frac{\partial p}{\partial z}+\mu\left[\frac{\partial^2 W}{\partial x^2}+\frac{\partial^2 W}{\partial y^2}+\frac{\partial^2 W}{\partial z^2}\right] \tag{8}$$

The turbulence viscosity is calculated using standard two equation (k-ε) turbulence model. The mesh at the inlet and outlet is with H-grid block and in the flow passage it is with O-grid block. Fine mesh at blade leading edge, trailing edge and near wall was imposed [20]. Periodicity is maintained by two symmetric surfaces positioned in the middle of blade passage as shown in Fig.1. The total numbers of elements, convergence criteria, boundary conditions etc are given in Table 3. The simulation has been performed on Intel Core 2 Duo having 2.93 GHz processor and 3 GB RAM. Approximately 15 hours of CPU time was required for each case.

3. RESULTS AND DISCUSSIONS

The flow rate, head and rotation of impeller comply with the corresponding specifications given in [4]. Simulated values for water as fluid, found to be in good agreement with that of the solutions given in the ref. [4]. The computations were carried out at different flow rates, i.e. at design and off-design conditions. The grid independency test was conducted for water at different flow rates. The pump head at design flow rate was taken as the parameter to evaluate grids and the influence of mesh size on solution was calculated by setting convergence criteria of 10^{-5}. Once the number of nodes reach a value of 560,000, the variation of head with the increase in number of nodes was not significant.

Table 3 Meshing and boundary conditions

Flow domain	Single impeller
Interface	Periodic
Mesh/Elements	Structural/568,620
Turbulence model	k-ε
Inlet/Outlet	Pressure/Mass flow rate
Residual convergence	$1x10^{-5}$
Residual type	RMS
Iteration steps	2000
Mass imbalance %	0.0001

Bradshaw [22] has reported that the selection of turbulence model was influenced by three issues: a) physical nature of problem, b) quality of attended results and c) computing power. Due to flow complexity the choice of turbulence model is delicate issue. In spite of this, the traditional models, like k-ε or k-ω are largely used and satisfactory results are achieved. The models k-ε, *SST* and k-ω were evaluated for impeller flow simulation, at design point and under similar conditions. The reference result [4] shows 40 m head at design flow rate, whereas by using k-ε, *SST* and k-ω turbulence models the values obtained were 43.51m, 43.95m and 45.15m, respectively. The least variation among these turbulence models was by k-ε and this model was used for further simulations. Three rotational speeds i.e. 1270 rpm, 1470 rpm and 1670 rpm were considered for the computations at deign and off design flow rates.

Figure 3 depicts the nature of the performance curves for the fluids. As D_2 is constant, any change in speed (N) leads to change in u_2 and this result to a change in the total head [19]. For this reason, higher head (H) at higher speed was obtained.

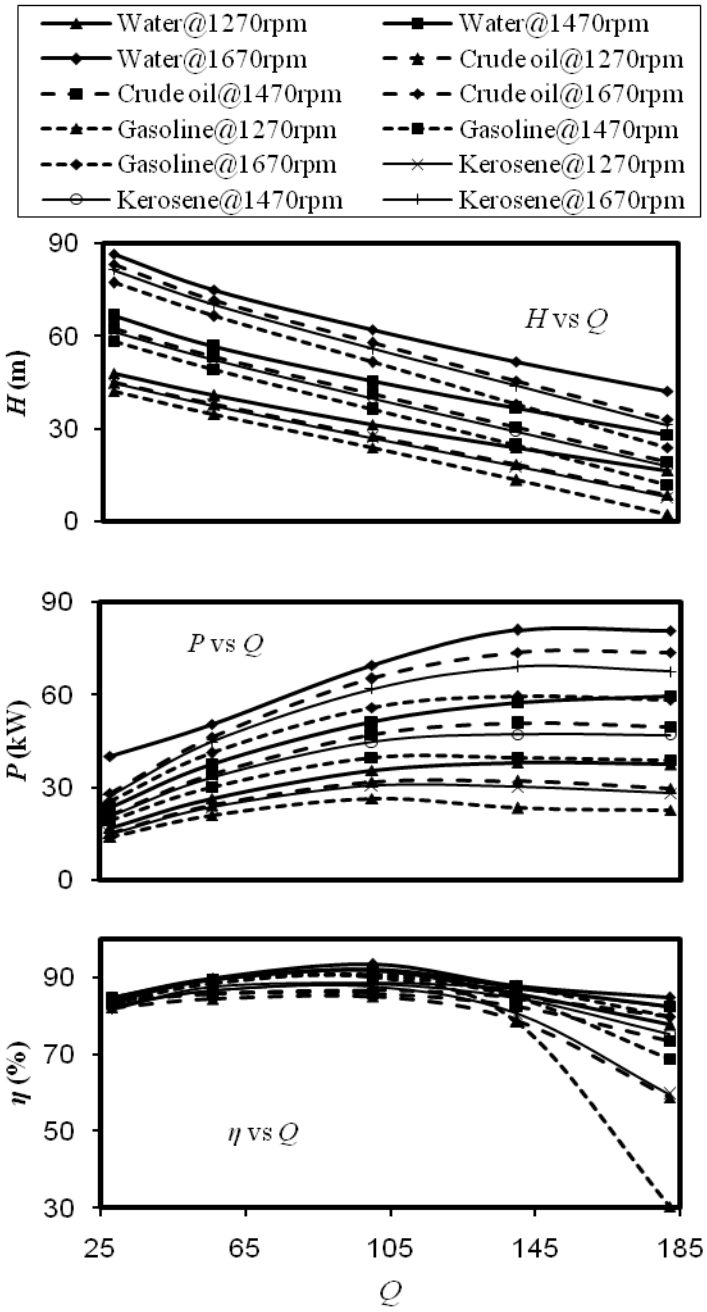

Fig. 3 Characteristics curves

From the results of 3D numerical analysis, total pressures at inlet (P_1) and outlet (P_2) was obtained and the head was calculated using the following equation:

$$H = \frac{P_2 - P_1}{\rho g} \tag{9}$$

Here H vs Q curve shifts parallelly upwards with respect the ref H-Q curve. Also equation (1) shows that the power consumption by the impeller is high at high flow rate. The density of crude oil, gasoline and kerosene is lesser than water which causes the lesser power consumption.

The hydraulic efficiency for the handling crude oil, gasoline and kerosene is lower than that for the handling water. The decrease in efficiency, while pumping the crude oil and saline-water is due to the viscosity which results in disc friction losses over the outsides of the impeller shroud and hub. These results show a good agreement with the analytical results of Gulich [23] and Li [14]. In addition to this, the head and discharge of the pump for which it was designed is at maximum efficiency point where hydraulic losses, profile losses and secondary losses were minimum. On the contrary at all other points of operation shock losses and secondary losses increase resulting into great hydraulic losses and decrease in hydraulic efficiency as well. But at low flow rates reverse flow and inlet recirculation are prominent and they increase with further reduction in flow rate. An increase in impeller speed leads to increase in total head [24]. Figure 3 represents variation in efficiency (η) curve with flow rate and the

curve is maximum for water at higher *N* at design flow rate. These results are in good agreement with that of Zhou *et al.* [1], Srinivasan [17] and Gulich [23].

Velocity distributions in between impeller vanes at off design are shown in Figures 4-5. The flow phenomena such as inlet recirculation, seperation in the impeller passage and exit recirculation is observed at low flow rates and this is reported in the literatures [6, 24-25].

Figures 4 demonstrate that at 0.25 Q_{design} and *N*= 1270, 1470 and 1670 rpm, both inlet recirculation and flow seperation in the impeller with reverse flow have been observed. At 0.25 Q_{design} and *N*=1270 rpm with zone-up view clearly depicts that inlet recirculation, flow seperation and reverse flow in impeller is existing (Fig. 4). This occurs as main flow enters at reduced flow rates, splits off, turn around and flows back into the inlet pipe near periphery. As reduced flow enters, seperation appears on the suction side of the blades (Fig. 4). This stagnant fluid in seperated region starts rotating in the impeller with centrifugal acceleration. The static pressure in this region is proportional to the square of the radius. It can be in the form of:

$$\frac{p}{\rho} = \frac{\omega^2 r^2}{2} \tag{10}$$

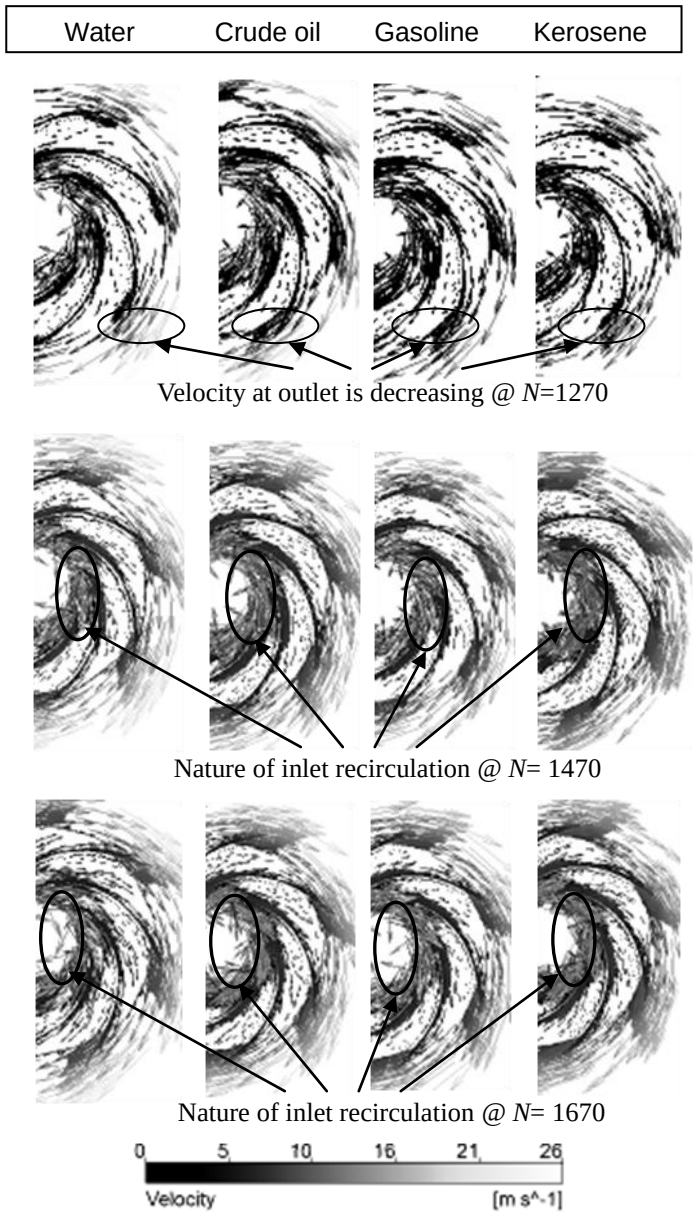

Fig. 4 Reverse flow and inlet recirculation at 0.25 Q_{design} and 50 % span

An alternate form of Bernoulli's equation for the rotating impeller in terms of relative velocity (*w*) known as rothalpy equation [21] can be written as;

$$I = \frac{p}{\rho g} + \frac{w^2}{2g} - \frac{\omega^2 r^2}{2g} \tag{11}$$

From inlet velocity triangle shown in Fig. 2 we can write;

$$w^2 = c_m^2 + \omega^2 r^2 \tag{12}$$

where, w and I are the relative velocity and rothalpy, respectively.

The meridional velocity c_m decreases with the radius. This is because of the quantity $\omega^2 r^2$ increases with radius and the relative velocity w remains constant. The separated region widens progressively with increase in radius and consequently blocks the inlet. Finally at the shroud with the greatest radius a stage is reached where the meridional velocity becomes zero. This occurrence is responsible and initiates inlet recirculation. As fluid particle progresses, flow pattern in impeller passage changes accordingly and results in the formation of reverse flow and flow separation. Once the flow approaches to Q_{design}, smooth flow is observed at inlet and in the impeller passage shown in Fig. 5. The velocity vectors at inlet and in impeller passage represent smooth flow and no separation of fluid is observed as reported by the researchers [5, 8, 25].

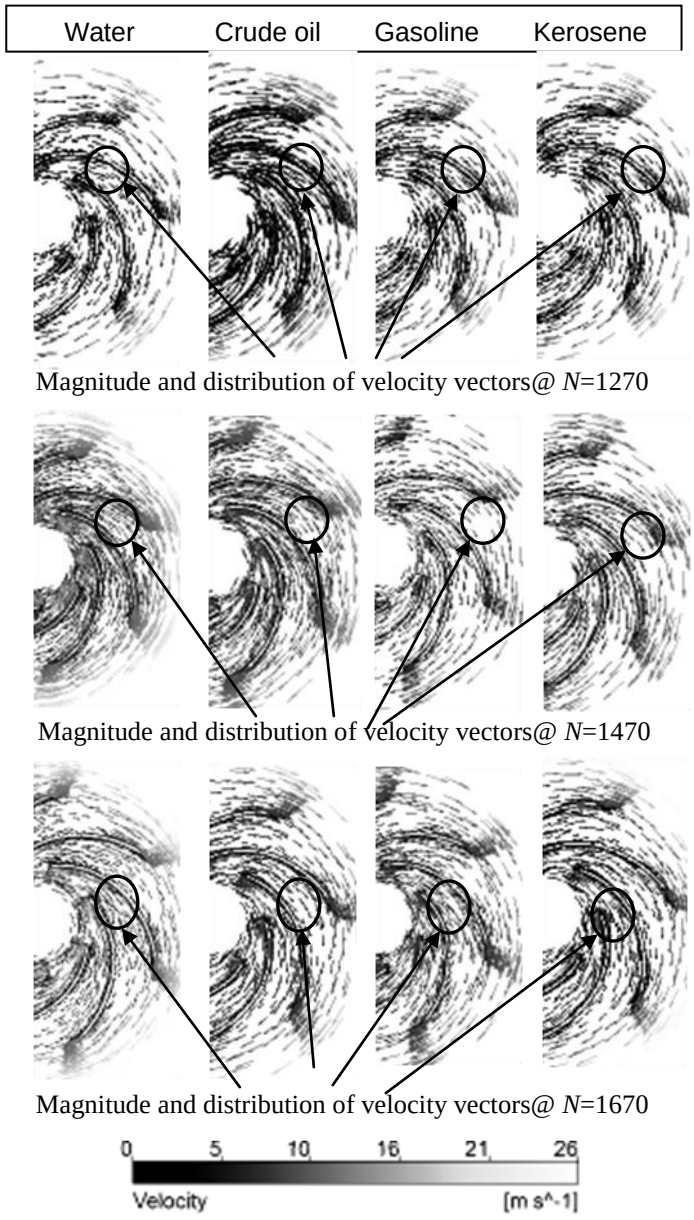

Fig. 5 Velocity vectors at Q_{design} and 50 % span

Figure 6 show the pressure contours on blade-to-blade plane for water, crude oil, gasoline and kerosene at 0.25 Q_{design}, and N=1270, 1470 and 1670 rpm. These figures clearly show that a marked zone of low pressure is developing at inlet of the impeller on suction side at off-design operation. The improper incidence shifts at low flow rate over to the vane suction surface creating a wake at the inlet as shown in Fig. 6. This wake establishes a zone prone to cavitation at leading edge on the suction surface. It is found that off-design operation is usually accompanied by cavitation [5, 17, 25]. Figure 7 represent the pressure contour on blade-to-blade plane for different fluids at Q_{design}. The pressure contours represents a smooth flow between the blades and its value increases continuously towards the exit of the computational domain. The figure depicts that the lowest static pressure observed at the impeller inlet on suction side. The highest static pressure occurs at the impeller outlet and the kinetic energy of flow reaches to maximum extent. Minimum pressure exists at the suction side and near the leading edge of the blade. This pressure distribution agrees the rotodynamic theory of pumps [5, 24]. But at 1.82 Q_{design} and N=1670 rpm, it is observed that apart from smooth flow in impeller passage a wake zone is established at impeller inlet on pressure side of the vane. This could be due to improper angle of incidence which the flow makes on the pressure side of the vane. This wake spreads more with increasing discharge leading to the formation of cavitation [21].

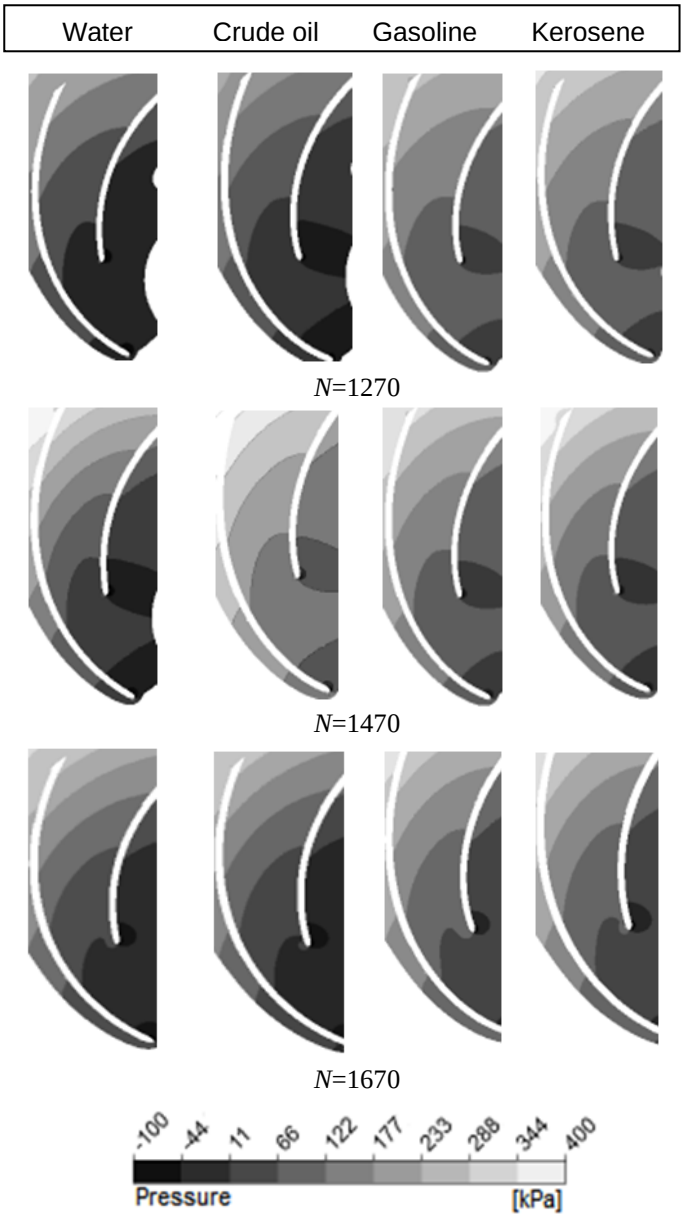

Fig. 6 Pressure contours at 0.25 Q_{design} and 50 % span

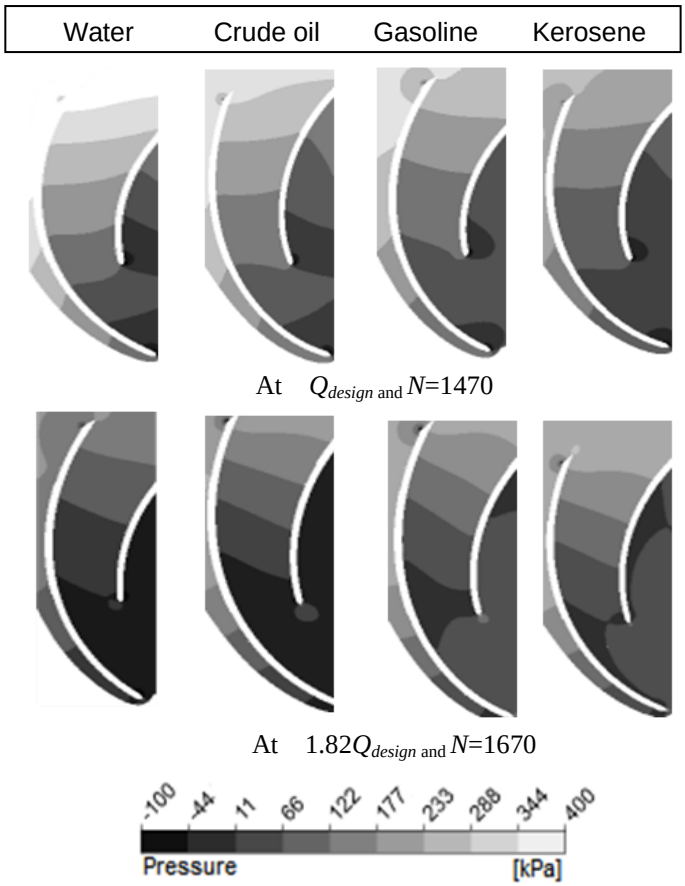

Fig. 7 Pressure contours at 50 % span

4. Conclusion

A centrifugal pump impeller performance for different liquids at design and off-design conditions has been evaluated by the numerical simulations. At low flow rate and at different impeller speeds, both inlet recirculation and flow seperation with reverse flow in the impeller passage have been observed. At design flow condition, a smooth flow between the blades is observed and its value increases continuously towards the exit of the flow domain. For low flow rate, the improper incidence shifts to the vane suction surface creating a wake at the inlet. The decrease in efficiency, while pumping the viscous fluids is due to the viscosity which results in disc friction losses outsides of the impeller shroud and hub. The work is going on to verify the numerical results with that of the experiments.

Acknowledgments

The authors would like to acknowledge Indian Institute of Technology Madras for the NFSC grant (Grant code: OEC/10-11/529/NFSC/ABDU) to conduct this research.

Nomenclature

CFD	Computational fluid dynamics
c	Absolute fluid flow velocity, m/s
g	Acceleration due to gravity, m/s^2
H	Head, m
ΔH	Hydraulic losses, m
h	Elevation from reference plane, m
I	Rothalpy, J/kg
N	Impeller speed, rpm
P	Power, W
p	Pressure, N/m^2
Q	Volume flow rate, m^3/s
RANS	Reynolds-averaged Navier Stokes
k	Turbulence kinetic energy, J
μ	Dynamic viscosity, N-s/m^2
R	Radius, m
SST	Shear stress transport
U	Velocity vector in x-direction
V	Velocity vector in y-direction
W	Velocity vector in z-direction
W	Relative fluid velocity, m/s

Greek Symbols

α	Flow angle, ^{o}
β	Blade angle, ^{o}
ε	Rate of energy dissipation, J/s
η	Hydraulic efficiency, %
a	Actual
design	Design flow

ρ	Density of fluid, kg/m^3	*h*	Hub
ω	Angular velocity, rad/s	*m*	Meridional component
		s	Shaft
	Subscript	*th*	Theoretical
1	Inlet	*u*	Peripheral component
2	Inlet		

References

[1] Zhou, W., Zhao, Z., Lee, T. S., and Winoto, S. H., 2003, "Investigation of flow through centrifugal pump impellers using computational fluid dynamics," International Journal of Rotating Machinery, Vol. 9, No. 1, pp. 49-61.
[2] Zhang, Y., Zhou, X., Ji, Z., and Jiang, C., "Numerical design and performance prediction of low specific speed centrifugal pump impeller," International Journal of Fluid Machinery and Systems, Vol. 4, No. 1, pp. 133-139.
[3] Stepanoff, A. J., 1964, Centrifugal and Axial Flow Pumps, 2nd Edition, John Wiley and Sons inc., New York.
[4] Lazarkiewicz, S., and Troskolanski, A. T., 1965, Impeller Pumps, 1st Edition, Pergamon Press Ltd., Oxford.
[5] Gulich, J. F., 2010, Centrifugal Pumps, 2nd Edition, Springer Publications, Berlin.
[6] Murakami, M., Kikuyama, K., and Asakura, E., 1980, "Velocity and pressure distributions in the impeller passages of centrifugal pump," ASME J. of Fluids Eng., Vol. 102, No. 4, pp. 420-426.
[7] Liu, C. H., Vafidis, C., and Whitelaw, J. H., 1994, "Flow characteristics of a centrifugal pump," ASME Journal of Fluids Eng., Vol. 116, No. 2, pp. 303-309.
[8] Akhras, A., El Hajem, M., Morel, R., and Champagne, J. Y., 2001, "Internal flow investigation of a centrifugal pump at the design point," Journal of Visualization, Vol. 4, No. 1, pp. 91-98.
[9] Abramian, M., and Howard, J. H. G., 1994, "Experimental investigation of the steady and unsteady relative flow in a model centrifugal impeller passage," ASME J. of Fluids Eng., No. 116, No. 2, pp. 269-279.
[10] Kaupert, K. A., and Staubli, T., 1999, "The unsteady pressure field in a high specific speed centrifugal pump impeller- Part I: Influence of the volute," ASME J. of Fluids Eng., Vol. 121, No. 3, pp. 621-626.
[11] Tsukamoto, H., Hata, S., Matsunaga, S., and Yoneda, H., 1986, "Transients characteristics of a centrifugal pump during stopping period," ASME J. of Fluids Eng., Vol. 108, No. 4, pp. 392-399.
[12] Li, W. G., and Hu, Z. M., 1997, "An experimental study on the performance of centrifugal oil pump," Fluids Machinery, Vol. 25, No. 2, pp. 3-7.
[13] Li, W. G., and Xue, D. S., 1998, "LDV measurement of viscous flow in a centrifugal pump impeller," Chinese Journal of Mechanical Engineering, Vol. 34, No. 6, pp. 97-101.
[14] Li, W. G., 2000, "Effects of viscosity on the performance of a centrifugal oil pump and the flow pattern in the impeller," International Journal of Heat and Fluid Flow, Vol. 21, No. 2, pp. 271-275.
[15] Li, W. G., and Xue, D. S., 2000, "Measurement of viscous oils flow in a centrifugal pump impeller," Chinese Journal of Mechanical Engineering, Vol. 36, No. 3, pp. 33-36.
[16] Fard, M. H. S., Boyaghchi, F. A., and M. B. Ehghaghi, 2006, "Experimental study and three-dimensional numerical flow simulation in a centrifugal pump when handling viscous fluids," IUST International Journal of Engineering Science, Vol. 17, No. 3, pp. 53-60.
[17] Srinivasan, K. M., 2008, Rotodynamic Pumps, New Age International (P) Ltd., New Delhi.
[18] Ansys-CFX 13.0., Ansys Inc., 2010.
[19] Wilcox, D. C., 1994, Turbulence Modeling for CFD, 2nd Edition, DCW Industries, Inc., La Canada, California.
[20] Desai, J., Chauhan, V., Charnia, S., and Patel, K., 2011, "Validation of Hydraulic Design of a Metallic Volute Centrifugal Pump using CFD," The 11th Asian International Conference on Fluid Machinery and 3rd Fluid Power Technology Exhibition, 21-23 Nov., pp. 1-8, IIT Madras, Chennai.
[21] Tuzson, J., 2000, Centrifugal Pump Design, 1st Edition, John Wiley and Sons, Inc., New York.
[22] Bradshaw, P., 1996, Turbulence modeling with application to turbomachinery, Progress in Aerospace Sciences, Vol. 32, No. 6, pp. 575-624.
[23] Gulich, J. F., 1999, "Pumping Highly Viscous Fluids with Centrifugal Pumps-Part 1," World pumps, Vol. 395, pp. 30-34.
[24] Gopalakrishnan, S., 1988, "A new method for computing minimum flow," Proceedings of the Texas A&M 5th International Pump User Symposium, Houston, Texas, pp. 41-47.
[25] Gopalakrishnan, G., and Prithviraj, D., 2011, A Treatise on Turbomachines, Scitech Publications (India) Pvt. Ltd., Chennai.